2022 American Control Conference (ACC)
Atlanta, USA, June 8-10, 2022

Autonomous Vehicle Overtaking in a Bidirectional Mixed-Traffic Setting

Faizan M. Tariq[1], Nilesh Suriyarachchi[1], Christos Mavridis[1] and John S. Baras[1]

***Abstract*— With the advent of autonomous vehicles on public roads imminent in the near future, special emphasis needs to be placed on addressing scenarios pertaining to mixed-traffic settings, comprised of human-driven and autonomous vehicles. In this paper, we address the problem of autonomous vehicle overtaking in a bidirectional mixed-traffic setting. We design a mixed-integer model predictive controller that maximizes the ego vehicle's velocity while prioritizing safety and accounting for driver comfort. The proposed approach: (i) operates in a limited sensing range while accounting for occlusion; (ii) is able to retract the overtake decision through a receding horizon approach; (iii) is robust to the variations in sensory input and driving behaviors of external agents due to behavior-dependent safety margins; and (iv) reduces to a mixed-integer optimization problem with linear constraints, yielding low computational complexity. We demonstrate the behavior of the proposed approach in a realistic traffic simulation environment.**

I. INTRODUCTION

In the pursuit of improving road safety by minimizing accidents caused by human error, autonomous vehicles will have to be introduced on public roads in the presence of existing human-driven vehicles. This presents numerous algorithmic challenges, especially in regards to robustness to the variations in human driving patterns [1]. The overtaking problem in a bidirectional mixed-traffic setting is a prime example that highlights these difficulties [2]. While fundamentally similar to the lane changing problem [3], the overtaking problem has added complexity due to the presence of incoming traffic, which increases the chances of head-on collisions. Moreover, the safety of overtaking maneuvers is highly contingent upon uncertainty factors such as road conditions, measurement accuracy, human driving behavior etc., making it a challenging problem to address.

Related Work

The approaches available in the literature to address the overtaking problem can be broadly classified into sampling-based, learning-based, and optimization-based methods. The sampling-based approaches typically involve sampling feasible trajectories from a reachable safe set, and are, therefore, able to incorporate non-holonomic constraints and safety guarantees [4]. However, the overall driving experience is often uncomfortable due to the concatenation of individual trajectories, and the asymptotic optimality guarantees do not translate to real-world implementability in complex driving scenarios due to high sample complexity [5].

[1]Electrical and Computer Engineering Department and the Institute for Systems Research, University of Maryland, College Park, Maryland, USA. Email: {mftariq,nileshs,mavridis,baras}@umd.edu

Research partially supported by ONR grant N00014-17-1-2622

The learning-based methods are among some of the most popular in the literature. Due to a lack of standardized dataset for the problem at hand, these approaches consist mainly of variations of reinforcement learning techniques trained in simulated environments [6]. Despite their seemingly good performance in simulations, the real-world implementations of these approaches raise a number of concerns (Sim2Real gap), such as the need for large amount of training data, exploration of unsafe behaviors, general inability to handle edge cases, and most importantly, the lack of explainability and safety guarantees as a consequence of utilizing neural networks as function approximators [7].

Lastly, the optimization-based approaches have been a standard in solving autonomous vehicle planning and control problems. The most prominent approaches in this area revolve around optimal control methods which are able to incorporate collision avoidance constraints while providing performance guarantees. However, they do so at a cost of high computational complexity, since they require solving an optimization problem on a functional space over a large time window, where the integration of non-linear dynamical models typically yields the additional bottleneck of non-convex constraints [8]. An efficient trade-off between performance guarantees and computational complexity is the Model Predictive Control (MPC) approach [9]. Many MPC variants have been proposed in the literature, such as Stochastic-MPC [10] and Robust-MPC [11], that allow for uncertainty considerations in the system dynamical model. However, these methods have not yet been applied to the bidirectional traffic flow setting. A promising exception in this regard is the recent work of Sulejmani et al. in [12], where a Stochastic-MPC method is applied in parallel with a Bayesian network to predict the trajectories of human driven vehicles. This approach, however, would require retraining of the network when used in different environments.

Contribution

In this paper, we address the autonomous vehicle overtaking problem in a bidirectional mixed-traffic setting. We design a model predictive controller that maximizes the ego vehicle's velocity while prioritizing safety and accounting for driver comfort. Our controller does not assume full knowledge of the environment and utilizes a realistic sensing and occlusion model instead. In regards to safety, we define variable safety margins, as functions of user-defined vehicle-specific attributes. Finally, the complexity of the receding horizon optimal control problem is reduced by introducing a binary decision variable to approximate the integrated

978-1-6654-5196-3/$31.00 ©2022 AACC

lateral dynamics of the ego vehicle, thus decoupling the longitudinal and lateral components of the dynamical model. As a result, the proposed approach is able to operate in a limited sensing range while accounting for occlusion, is able to retract the overtake decision through the receding horizon approach, is robust to variations in sensory input and driving behaviors of external agents, and reduces to a mixed-integer optimization problem with linear constraints yielding low computational complexity. We evaluate the efficacy of the proposed approach in a widely used simulation environment.

Notation

Throughout the manuscript, $\mathbb{N}$ will denote the set of non-negative integers and $\mathbb{R}$ the set of real numbers. For some $a, c \in \mathbb{N}$ and $a < c$, we will write $\mathbb{N}_{[a,c]} = \{b \in \mathbb{N} \mid a \leq b \leq c\}$. For some $e, g \in \mathbb{R}$ and $e < g$, we will write $\mathbb{R}_{[e,g]} = \{f \in \mathbb{R} \mid e \leq f \leq g\}$. Whenever $<, \leq, =, \geq, >$ are applied to vectors, they are interpreted element-wise.

II. Problem Formulation

A scenario with three types of vehicles is considered: autonomous ego vehicle, vehicle(s) traveling ahead in the same lane as the ego vehicle and the incoming vehicle(s) in the adjacent lane. No restriction is placed on the class of non-ego vehicles such that they can be human-driven or autonomous. The goal of the ego vehicle is to travel at its maximum safe velocity and when required, safely overtake the vehicle(s) traveling ahead. The term safety encompasses respecting ego vehicle's design (state, control and actuation) limits, real-time operation, maintaining safe distances to the neighboring vehicles and obeying traffic rules (staying within lanes and not exceeding speed limits). The typical vehicle trajectories in a three-vehicle scenario are depicted in Fig. 1.

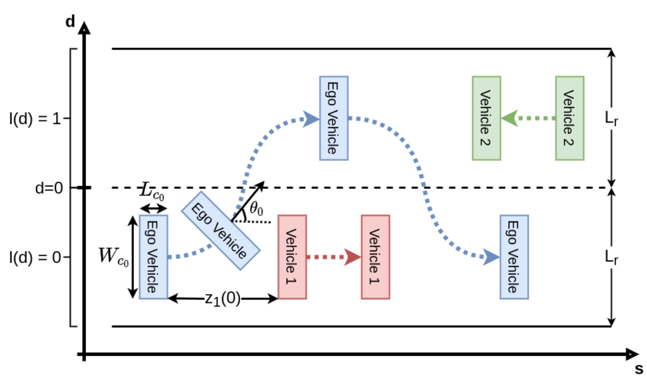

Fig. 1. Problem Overview

A. Road Model

The width of each of the lanes is denoted by L_r and the speed limit by V_l. Let the global Frenet coordinate frame be centered at the left-end of the lane divider. The Frenet coordinate frame is composed of two variables: longitudinal displacement (s) and lateral displacement (d). The binary variable l distinguishes between the two lanes such that $l(d) = \mathbb{1}_{d \geq 0}$. All introduced variables are depicted in Fig. 1.

B. Vehicle Dynamics

Let $t \in \mathbb{R}_{\geq 0}$ denote the time variable and $\mathbb{V}(t) = \{x_i(t) \in \mathbb{X} \mid i \in \mathbb{N}_{[0,n]}\}$ denote the set of states of the vehicles present in the environment at time instant t. The state x_i is comprised of longitudinal displacement (s_i), lateral displacement (d_i) and heading angle (θ_i), represented compactly as:

$$x_i(t) = [s_i(t), d_i(t), \theta_i(t)]^\top \in \mathbb{X} \tag{1}$$

where

$$\mathbb{X} = \{z \in \mathbb{R}^3 \mid [-\infty, -L_r, -\pi]^\top \leq z \leq [\infty, L_r, \pi]^\top\}$$

represents the physical limits on the state variables. The index $i = 0$ identifies the ego vehicle while $i \in \mathbb{N}_{[1,n_0]}$ and $i \in \mathbb{N}_{[n_0+1,n]}$ denote the vehicles, excluding the ego vehicle, traveling in lanes $l(d(t)) = 0$ and $l(d(t)) = 1$, respectively. We define $n_1 = |\mathbb{N}_{[n_0+1,n]}| = n - n_0$. For simplicity, and without affecting any safety guarantees (Section III-C), the vehicles are physically modeled as rectangles with the length and width of vehicle i defined as L_{c_i} and W_{c_i}, respectively, as shown in Fig. 1.

1) Ego Vehicle Dynamics Model: With the sampling period denoted by T_s, the discretized dynamics of the ego vehicle are modeled by the non-holonomic unicycle (*Dubins*) model, as follows:

$$s_0(k+1) = s_0(k) + v_0(k) \cdot \cos(\theta_0(k)) \cdot T_s \tag{2}$$
$$d_0(k+1) = d_0(k) + v_0(k) \cdot \sin(\theta_0(k)) \cdot T_s \tag{3}$$
$$\theta_0(k+1) = \theta_0(k) + \omega_0(k) \cdot T_s \tag{4}$$

where $s_0(0) = 0$, $d_0(0) = -L_r/2$, $\theta_0(0) = 0$, and $k \in \mathbb{N}_{\geq 0}$. Here, the longitudinal velocity (v_0) and angular velocity (ω_0) are the control variables, represented compactly as:

$$u_0(k) = [v_0(k), \omega_0(k)]^\top \in \mathbb{U}(u_0(k-1), T_s) \tag{5}$$

where

$$u_0(0) = [0, 0]^\top, \text{ and}$$
$$\mathbb{U}(a, T_s) = \{z \in \mathbb{R}^2 \mid [0, \omega_{min}]^\top \leq z \leq [V_{max}, \omega_{max}]^\top, \; [A_{min}, \alpha_{min}]^\top \leq \frac{z - a}{Ts} \leq [A_{max}, \alpha_{max}]^\top\}.$$

Here, $\mathbb{U}(u_0(k-1), T_s)$ represents the physical limits on control inputs at time instant k. V_{max} denotes the maximum reachable linear velocity of the ego vehicle while ω_{min} and ω_{max} denote the minimum and maximum reachable angular velocity of the ego vehicle. The linear velocity, $v_0(k)$, is lower bounded by 0 because reversing behavior is not permitted on a highway. Moreover, bounds are placed on the actuation limits by defining the admissible linear and angular accelerations. Here, A_{min} and A_{max} correspond respectively to the maximum linear deceleration and acceleration while α_{min} and α_{max} correspond respectively to the maximum angular deceleration and acceleration of the ego vehicle.

2) Observed Vehicles' Dynamics Model: The dynamics of the observed vehicles are modeled using the linearized unicycle (*Dubins*) model around the trajectory defined by $\theta(k) = 0$, as follows:

$$\begin{aligned} s_i(k+1) &= s_i(k) + v_i(k) \cdot T_p + \tilde{n}_{v_i}(k) \\ d_i(k+1) &= d_i(0) \\ \theta_i(k+1) &= \theta_i(0) \end{aligned} \tag{6}$$

for all $i \in \mathbb{N}_{[1,n]}$, where $v_i(k) \in \mathbb{R}_{[0,V_{max}]}$, $\theta_i(0) = 0$, $\tilde{n}_{v_i}(k) \sim \mathcal{N}(0, \sigma_v^2)$, and $d_i(0) = \begin{cases} -\frac{L_r}{2}, & i \in \mathbb{N}_{[1,n_0]} \\ \frac{L_r}{2}, & i \in \mathbb{N}_{[n_0+1,n]} \end{cases}$. Here, T_p corresponds to the observation sampling period and $\tilde{n}_{v_i}$ corresponds to the noise in the dynamics model. Notice that the observation sampling period is denoted by a separate variable T_p to indicate that it need not be the same as the discretization sampling period T_s, introduced in Section II-B. This distinction will play an important role in Section III-A.

C. Sensing Model

1) Measurement variables: Utilizing data from the on-board sensor suite, state-of-the-art sensor fusion algorithms [13] are able to obtain the relative displacement of vehicles present in the vicinity of the ego vehicle with a high degree of accuracy. Based on the availability of sensor data, we formulate the problem in terms of the relative displacements $z_i(k)$ of the set of observed vehicles $\{i : x_i \in \mathbb{O}\}$, defined in Section II-C.2. The noisy observation measurements $\tilde{z}_i(k)$ are defined in a moving coordinate system centered at the ego-vehicle at any time instant k as follows:

$$\tilde{z}_i(k) = z_i(k) + \tilde{n}_{s_i} = s_i(k) - s_0(k) + \tilde{n}_{s_i} \tag{7}$$

where $\tilde{n}_{s_i} \sim \mathcal{N}(0, \sigma_s^2)$, and $\tilde{z}_i(k) \in \mathbb{R}_{[-L_s,L_s]}$. Here, L_s corresponds to the measurement range of the ego vehicle's on-board sensor suite and $\tilde{n}_{s_i}$ corresponds to the noise in the measurement variables. The additive uncorrelated Gaussian noise model for the measurement noise is justified by the experimental results that show good real-world performance for 3D LiDAR data under this modeling assumption [14].

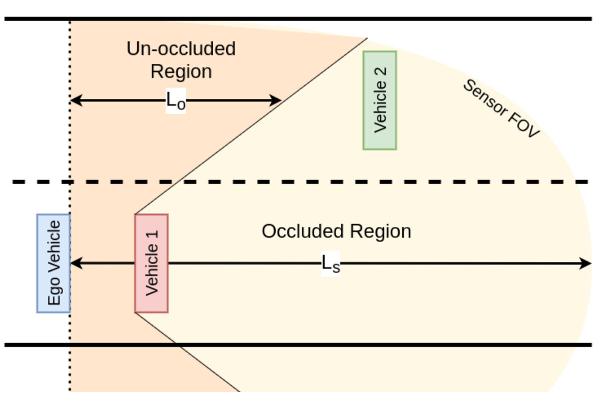

Fig. 2. Occlusion

2) Occlusion: To account for occlusion, we model the limited sensor visibility in the adjacent lane in presence of a leading vehicle. This is done by introducing an alternate measurement range $L_o < L_s$, shown in Fig. 2, that defines the maximum longitudinal displacement at which a vehicle can be observed in the adjacent lane when a leading vehicle is present within the measurement range L_s. In practice, L_o can be a function of headway (distance to the leading vehicle), but for the scope of this work, it is assumed to be constant. We take the value of L_o as the worst-case measurement range for the adjacent lane i.e. the visibility range in the adjacent lane when the leading vehicle is traveling at the minimum allowable safety margin L_{0_1} (see Section III-B.1). Then, the ego vehicle's observation state set is defined as:

$$\begin{aligned} \mathbb{O}_0(k) = \min_{0 \le z_i(k) \le L_s} \{ & x_i(k) \in \mathbb{V}(k) \setminus \{x_0(k)\} \mid \\ & (l(d_i(k)) = l(d_0(k)) \} \end{aligned} \tag{8a}$$

$$\begin{aligned} \mathbb{O}_1(k) = \{ & x_i(k) \in \mathbb{V}(k) \setminus \{x_0(k)\} \mid \\ & (l(d_i(k)) \neq l(d_0(k)) \cap (|z_i(k)| \le L_o) \} \end{aligned} \tag{8b}$$

$$\mathbb{O}(k) = \mathbb{O}_0(k) \cup \mathbb{O}_1(k) \tag{8c}$$

At any time instant k, the set of states of the observed vehicles is denoted by $\mathbb{O}(k)$, as shown in (8c). For the vehicles traveling in the same lane as itself, the ego vehicle is able to observe the vehicle in its direct line of sight given that it falls within the measurement range L_s, as shown in (8a). As for the vehicles traveling in the adjacent lane, the ego vehicle is able to observe all the vehicles in the un-occluded region, defined by L_o, as shown in (8b).

III. Methodology

In this section, we describe a state estimation mechanism based on Kalman filtering, define the main optimal control problem, and prove the existence of a feasible solution that respects all the defined safety constraints.

A. State Estimation

The ego vehicle estimates the relative longitudinal displacement $\hat{s}_i(k)$ of the vehicles with states in the observation state set $\mathbb{O}(k)$ based on the longitudinal dynamics model (6) and the measured longitudinal displacement (7). Let the estimated relative longitudinal displacement and the estimated covariance at time instant k for the vehicle i be defined as $\hat{s}_i(k)$ and $\hat{\Sigma}_i(k)$ respectively. Then, for all $k > 0$ and $i \in \mathbb{N}_{[1,n]}$ such that $x_i \in \mathbb{O}(k)$, $\hat{s}_i(k)$ and $\hat{\Sigma}_i(k)$ can be estimated using a Kalman filter [15] as follows:

$$\tilde{u}_i(k) = \frac{\hat{s}_i(k-1) - \hat{s}_i(k-2)}{T_p} \tag{9}$$

$$\begin{aligned} \tilde{s}_i(k) = {} & A_i(k) \cdot \hat{s}_i(k-1) + B_i(k) \cdot \tilde{u}_i(k) \\ & - (s_0(k) - s_0(k-1)) \end{aligned} \tag{10}$$

$$\tilde{\Sigma}_i(k) = A_i(k) \cdot \hat{\Sigma}_i(k-1) \cdot A_i^\top(k) + R_i(k) \tag{11}$$

$$K_i(k) = \frac{\tilde{\Sigma}_i(k)}{\tilde{\Sigma}_i(k) + Q_i(k)} \tag{12}$$

$$\hat{s}_i(k) = \tilde{s}_i(k) + K_i(k) \cdot (\tilde{z}_i(k) - \tilde{s}_i(k)) \tag{13}$$

$$\hat{\Sigma}_i(k) = (1 - K_i(k)) \cdot \tilde{\Sigma}_i(k) \tag{14}$$

where $\hat{s}_i(q) = \tilde{z}_i(q)\ \forall q \in \{0,1\}$, $\hat{\Sigma}_i(0) = R_i(k) = {\sigma_{v_i}}^2$, $Q_i(k) = {\sigma_{s_i}}^2$, $A_i(k) = 1$, $B_i(k) = \begin{cases} T_p, & i \in \mathbb{N}_{[1,n_0]} \\ -T_p, & i \in \mathbb{N}_{[n_0+1,n]} \end{cases}$. Since the estimator sampling time T_p is independent of the controller sampling time T_s, the estimator can be run at a much higher frequency as compared to the controller because the linear recursive updates of the estimator have low computational complexity. This difference in frequency updates is a known property of dynamic observer design that helps establish practical convergence of the estimated observations to the actual ones.

B. Optimal Control Problem

The optimal control objective is to determine a sequence of velocity commands that would enable the ego vehicle to maximize its velocity while respecting its dynamics, actuator limits and safety constraints. In a highway overtaking scenario, where the road curvature is small, it is reasonable to assume that the longitudinal and lateral dynamics of the ego vehicle are decoupled [16]. Moreover, given an adequate longitudinal safety margin, the existing low-level vehicle controllers are able to efficiently perform lane change maneuvers while abiding by lateral dynamical constraints [17]. Under these premises, we introduce a hierarchical controller architecture composed of a high-level central controller and a low-level lateral controller. The central controller handles the high-level decision making based on estimated longitudinal measurements and provides commands to the lateral controller that governs the low-level lateral movements.

1) Central controller: The central controller makes use of a binary decision variable $\mathcal{D}(k)$ to abstract out the lateral dynamics. This allows for a decoupling of longitudinal and lateral dynamics, and controllers, which in turn leads to an overall reduction in computational complexity, as evident in the timing statistics provided in Section IV.

Let the decision to overtake at any time instant k, be denoted by $\mathcal{D}(k) \in \{0,1\}$. Here, $\mathcal{D}(k) = 1$ corresponds to the decision to travel in the adjacent lane ($l(d(k)) = 1$) while $\mathcal{D}(k) = 0$ represents the decision to travel in the original lane ($l(d(k)) = 0$). With the lateral component of the dynamics model in Section II-B.1 represented by the binary decision variable, the decoupled longitudinal dynamics model linearized around the trajectory $\theta(k) = 0$ is posed as follows:

$$\bar{x}(k+1) = \bar{x}(k) + \bar{u}(k) \cdot T_s \tag{15}$$

where $\bar{u}(k) \in \bar{\mathbb{U}}(\bar{u}(k-1), T_s) = \{z \in \mathbb{R}_{[0,V_l]} \mid A_{min} \leq \frac{z-\bar{u}(k-1)}{Ts} \leq A_{max}\}$, $\bar{x}(0) \in \mathbb{R}_{[-\infty,\infty]}$, and $\bar{u}(0) \in \mathbb{R}_{[0,V_l]}$. Here, $\bar{x}(k)$ and $\bar{u}(k)$ correspond to the longitudinal displacement and velocity, respectively, while $\bar{\mathbb{U}}(\bar{u}(k-1), T_s)$ encompasses the actuator limits.

The central controller is posed as a mixed-integer MPC (MI-MPC) that outputs the binary decision $\mathcal{D}(k+1)$ and the control input $v_0(k+1)$, at time instant k. The goal is to maximize the velocity of the ego vehicle, minimize the time spent in the adjacent lane and penalize abrupt changes in velocity while satisfying vehicle limits and safety constraints. The optimization problem is defined as follows:

$$\begin{aligned} \min_{\substack{\bar{u}^k(1),\cdots,\bar{u}^k(H);\\ \mathcal{D}^k(1),\cdots,\mathcal{D}^k(H)}} \quad & \sum_{j=1}^{H} [-\gamma_1 \cdot \bar{u}^k(j) + \gamma_2 \cdot \mathcal{D}^k(j) \\ & + \gamma_3 \cdot (\bar{u}^k(j) - \bar{u}^k(j-1))^2] \end{aligned} \tag{16}$$

$$\text{s.t.} \quad \bar{x}^k(0) = 0 \tag{17}$$

$$\bar{u}^k(0) = \bar{u}(k) \tag{18}$$

$$\forall j \in \{1, \cdots, H\}:$$

$$\bar{x}^k(j+1) = \bar{x}^k(j) + \bar{u}^k(j) \cdot T_s \tag{19}$$

$$\bar{x}^k(j) \in \mathbb{S}(j) \tag{20}$$

$$\bar{u}^k(j) \in \bar{\mathbb{U}}(\bar{u}^k(j-1), T_s) \tag{21}$$

$$\mathcal{D}^k(j) \in \{0,1\} \tag{22}$$

In the formulated optimization objective (16), the tradeoff parameters γ_1, γ_2 and γ_3 govern the tradeoff between maximizing velocity, minimizing time spent in the adjacent lane and minimizing abrupt changes in velocity between consecutive time steps. Increasing parameter γ_1 yields a more aggressive behavior with a higher emphasis placed on achieving maximum velocity at the expense of driver comfort while parameters γ_2 and γ_3 emphasize driver comfort by reducing lane and velocity changes, respectively, while sacrificing velocity gains. The output of the optimization at time instant k is $\{\bar{u}_*^k(1), \cdots, \bar{u}_*^k(H), \mathcal{D}_*^k(1), \cdots, \mathcal{D}_*^k(H)\}$ which is applied in a receding horizon fashion.

2) Safety Constraints: At any planning instant j, the ego vehicle needs to maintain vehicle dependent longitudinal safety margins to the vehicles traveling in its lane. This is compactly represented as follows:

$$\begin{aligned} \mathbb{S}_0(j) = \{ & z \in \mathbb{R} \mid \\ & (1 - \mathcal{D}^k(j)) \cdot (|\hat{s}_i(j) - z| - (L_{c_i} + L_{sm_i}(k))) \geq 0, \\ & \forall i \in \mathbb{N}_{[1,n_0]} \ni x_i \in \mathbb{O}(k)\} \end{aligned} \tag{23}$$

$$\begin{aligned} \mathbb{S}_1(j) = \{ & z \in \mathbb{R} \mid \\ & \mathcal{D}^k(j) \cdot (|\hat{s}_i(j) - z| - (L_{c_i} + L_{sm_i}(k))) \geq 0, \\ & \forall i \in \mathbb{N}_{[n_0+1,n]} \ni x_i \in \mathbb{O}(k)\} \end{aligned} \tag{24}$$

$$\mathbb{S}(j) = \mathbb{S}_0(j) \cup \mathbb{S}_1(j) \tag{25}$$

Here, the safe set $\mathbb{S}(j)$ represents the set of longitudinal coordinates deemed safe for the ego vehicle to be in at planning instant j and $L_{sm_i}(k)$ corresponds to the longitudinal safety margin that the ego vehicle needs to maintain from vehicle i for the entirety of the planning horizon at time instant k, which is defined as follows:

$$\begin{aligned} L_{sm_i}(k) = & L_{0_i} + \frac{L_{v_i}}{V_l} \cdot \tilde{u}_i(k) + \frac{L_{a_i}}{A_{max}} \cdot \frac{|\tilde{u}_i(k) - \tilde{u}_i(k-1)|}{T_s} \\ & + \mathbb{1}_{i \in \mathbb{N}_{[n_0+1,n]}} \cdot \frac{L_{l_i}}{V_l} \cdot (\bar{u}(k) + \tilde{u}_i(k)) \end{aligned} \tag{26}$$

The safety margin $L_{sm_i}(k) \in \mathbb{R}_{>0}$ for vehicle i at time instant k depends on its estimated control input (longitudinal velocity, Section III-A); the change in its estimated control input between sampling time steps (longitudinal acceleration); and the summation of its estimated control input with the ego vehicle's own control input (relative longitudinal velocity) for the incoming vehicles. Here, $L_{0_i} \in \mathbb{R}_{>0}$ corresponds to the minimum nominal safety margin that needs to be maintained regardless of the behavior of vehicle i while $L_{v_i} \in \mathbb{R}_{>0}$, $L_{a_i} \in \mathbb{R}_{>0}$ and $L_{l_i} \in \mathbb{R}_{>0}$ correspond respectively to the multiplicative factors associated with velocity, acceleration and lane of vehicle i. The safety margin parameters are all vehicle dependent since different types of vehicles (car, truck, bike etc.) require different nominal safety margins and multiplicative factors. The modification of safety margin with the behavior of the corresponding vehicle allows the controller to perform optimally regardless of varying driver patterns, as validated in Section IV-B.3.

Remark 1: In contrast to the existing work [18], [19], the proposed approach estimates the driving behavior of a vehicle from observations rather than having it as a user-defined parameter, which results in a reactive control strategy.

Remark 2: The safety margins (L_{0_i}, L_{v_i}, L_{a_i} and L_{l_i}) are fine-tuned empirically based on the ego vehicle's dynamical constraints and the operational design domain (ODD) specifications, allowing for varying level of conservativeness.

Remark 3: The decision-making system does not explicitly account for the time required by the lateral controller to execute its desired decision. This is by design, since the ego vehicle may be able to observe the initially occluded vehicle(s) by nudging into the adjacent lane and potentially retract its decision thereafter without having to move all the way to the center of the adjacent lane. Moreover, this also allows for the decision-making system to be made completely independent of the choice of the lateral controller, as long as L_{0_i} has been tuned appropriately (i.e. chosen large enough to accommodate the longitudinal distance covered while changing lanes) for the controller at hand.

3) Safety constraint implementation: The safety constraints posed in (23) and (24) do not belong to the standard form of a mixed integer quadratic program [20]. In order to convert the constraints into the standard linear form, the big-M method [21] is applied as follows:

$$(23) \iff \begin{cases} (\hat{s}_i(j) - z + M \cdot a(j) - \\ (L_{c_i} + L_{sm_i}(k))) + N_1 \cdot \mathcal{D}^k(j) \geq 0 & \text{(27a)} \\ -(\hat{s}_i(j) - z - M \cdot (1 - a(j)) + \\ (L_{c_i} + L_{sm_i}(k))) + N_1 \cdot \mathcal{D}^k(j) \geq 0 & \text{(27b)} \end{cases}$$

$$(24) \iff \begin{cases} (\hat{s}_i(j) - z + M \cdot b(j) - (L_{c_i} \\ + L_{sm_i}(k))) + N_2 \cdot (1 - \mathcal{D}^k(j)) \geq 0 & \text{(28a)} \\ -(\hat{s}_i(j) - z - M \cdot (1 - b(j)) + (L_{c_i} \\ + L_{sm_i}(k))) + N_2 \cdot (1 - \mathcal{D}^k(j)) \geq 0 & \text{(28b)} \end{cases}$$

where $M, N_1, N_2 \gg 0$, and $a(k), b(k) \in \{0, 1\}$. The constants N_1 and N_2 allow for automatic satisfaction of the inactive constraints out of (23) and (24), based on the value of $\mathcal{D}^k(j)$, thus removing the quadratic terms. The constant M, in conjunction with the boolean variables $a(k)$ and $b(k)$, responsible for accommodating the sign of the absolute value term, allows for the transformation of the absolute value constraint into two linear ones. Therefore, the linear constraints (27a)-(28b) are used as safety constraints in the implementation of the central controller.

4) Lateral Controller: The proposed approach can work in conjunction with any lane-changing model and lateral controller found in the literature [22], [23], [24], given that the low-level controller does not significantly alter the longitudinal dynamics. An example of such a decoupled lateral controller is provided in [10]. In this work, without loss of generality, we make use of a simple, yet sufficiently effective (Section IV), lateral controller represented by the filtering of the decision signal $\mathcal{D}(k)$ by a moving average (FIR) low-pass filter with a given window size N, as follows:

$$d_0(k) = \frac{L_r}{N} \sum_{n=0}^{N-1} \mathcal{D}(k-n) - \frac{L_r}{2}. \tag{29}$$

C. Feasibility Analysis

Theorem 1: Suppose that $L_o > \dfrac{2V_{max}^2}{-A_{min}} + L_{sm}^{max}$, where L_{sm}^{max} is the maximum possible safety margin, based on the chosen parameters, and $\forall i \in \mathbb{N}_{[0,n]}$, $\tilde{n}_{v_i}(k) = \tilde{n}_{s_i}(k) = 0$, $\tilde{u}_i(k) = v_i(k) = v_i(0)$. If $s_i(0)$ is such that the problem (Section III-B.1) is initially feasible at $k = 0$, with $\mathcal{D}_0^*(1) = 0$, then under the assumption of self-preserving agents [25], it remains feasible for all $k \geq 0$.

Proof: Given the conditions of *Theorem 1*, a feasible solution that holds for all $k > 0$, in the presence of a leading vehicle, is as follows:

$$\bar{u}^k(j) = \begin{cases} \tilde{u}_a(k), & \Delta u(j) \geq A_{min} \cdot Ts \\ & \Delta u(j) \leq A_{max} \cdot Ts \\ \bar{u}^k(j) + A_{max} \cdot Ts, & \Delta u(j) \geq A_{max} \cdot Ts \\ \bar{u}^k(j) - A_{min} \cdot Ts, & \Delta u(j) \leq A_{min} \cdot Ts \end{cases} \tag{30}$$

$$\mathcal{D}^k(j) = 0 \tag{31}$$

for all $j \in \{1, \cdots, H\}$, where $\Delta u(j) = \tilde{u}_a(k) - \bar{u}^k(j)$, $a \in \mathbb{N}_{[1,n]}$ such that $x_a(0) \in \mathbb{O}_0(0)$. ■

Remark 4: The conditions in *Theorem 1* are required for completeness purposes since there exist scenarios such as ill-posed initialization or relying on faulty sensors, resulting in $|\tilde{n}_{s_i}(k)| \gg 0$ (measurements dominated by noise) or $L_s \approx 0$ (no visibility), that may lead to infeasibility.

IV. Experimental Results

The performance of the proposed approach is evaluated in a bidirectional closed loop road simulation, allowing the traffic to be continuously rerouted, so that the long-term behavior of the proposed approach can be evaluated.

This is an important consideration, especially in the case of high-density traffic, since a long-duration simulation can reveal corner-cases that may go unnoticed in a short-term simulation of a single overtake maneuver that is often utilized in existing works [18], [19], [22].

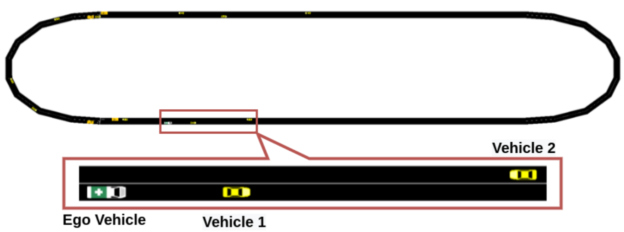

Fig. 3. Simulation Environment in SUMO

The simulation is implemented in the SUMO environment [26], shown in Fig. 3. The Gurobi Optimizer (Version 9.1.1) [27] is used to solve the mixed-integer quadratic programming (MIQP) problem posed in Section III-B, at every sampled time instant T_s. The controller communicates with the simulator using SUMO's built-in traffic controller interface (TraCI). The simulation and optimization algorithms are both implemented on a personal computer equipped with an Intel i7-4710HQ CPU with 16GB of RAM running Ubuntu 18.04. We note that the average time required for each optimization step is $11.246\,ms$ with a standard deviation of $0.233\,ms$. For reference, the reaction time of a human driver is $2.3\,s$ [28], and a vehicle with a speed of $60\,m/h$ covers $0.2682\,m$ in $10\,ms$. This suggests that the proposed approach is suitable for real-time use in real-world scenarios. Notice that the running time of about 10ms is achieved on an average personal computer and can be further reduced by the use of dedicated hardware.

Simulation Parameters	**Value**
Simulation step size	100 ms
Simulation duration	1 hour
Road length	1 km
Road speed limit (V_l)	20 m/s
Other vehicles' speed ($v_i(k) : \forall i \neq 0, \forall k$)	10 m/s
Vehicles' length ($L_{ci} : \forall i$)	5 m
Vehicles' width ($W_{ci} : \forall i$)	2.16 m
Controller Parameters	**Value**
Controller sampling time (T_s)	500 ms
Maximum acceleration (A_{max})	6 m/s^2
Maximum deceleration (A_{min})	-9 m/s^2
Maximum velocity (V_{max})	30 m/s
Normal sensing range (L_s)	150 m
Occluded sensing range (L_o)	75 m
Planning horizon (H)	10 s
Safety Margin Parameters ($[L_{0_i}, L_{v_i}, L_{a_i}, L_{l_i}]$)	[10, 5, 5, 10]

TABLE I
SIMULATION & CONTROLLER PARAMETERS

A. Simulated Trajectories

The behavior of the ego vehicle during an overtake scenario involving five vehicles is illustrated in Fig. 4. The simulation and the controller parameters are outlined in Table I. The ego vehicle can initially detect two vehicles in its sensing range: a leading vehicle in the same lane (Vehicle 1) and an incoming vehicle in the adjacent lane (Vehicle

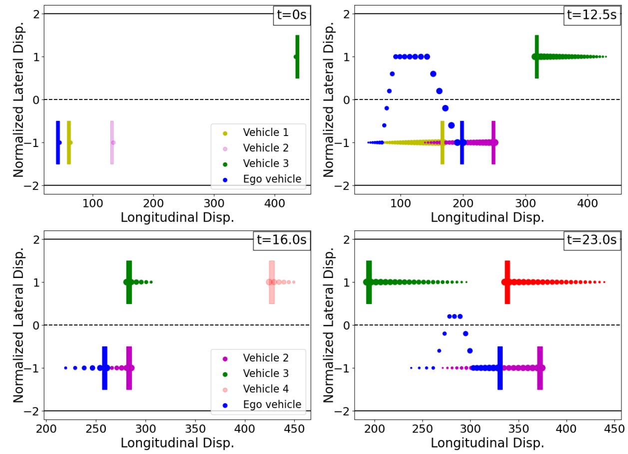

Fig. 4. Vehicle trajectories

3). Note that the initially occluded (depicted in a lighter shade) Vehicle 2 comes into the ego vehicle's sensing range after initiating the overtake maneuver. After successfully overtaking Vehicle 1, the ego vehicle is able to sense another leading vehicle (Vehicle 2) while still having Vehicle 3 in its sensing range. After waiting for the Vehicle 3 to pass, the ego vehicle starts another overtake maneuver. After initiating the maneuver, an additional incoming vehicle in the adjacent lane (Vehicle 4) enters the ego vehicle's sensing range (unoccluded region), and the overtake decision is retracted.

This result highlights the importance of active perception in autonomous driving. That is, for a safe controller to be used in real-world settings, perception and control cannot be assumed independent. Rather, taking an action, e.g., starting the process of overtaking, can result in better sensory input which should be used to alter the decision of the vehicle online. One important detail, which is often overlooked, is that the action that leads to new observations, such as the one presented above, must be safe. This is, therefore, different from the way reinforcement learning algorithms are trained [7], and is availed to us by the proposed MPC approach, detailed in Section III-B.1.

B. Performance Metrics

We analyze the performance of the proposed approach by considering the effects of different parameters on the following performance metrics, computed over a long-term simulation, in the closed loop environment shown in Fig. 3:

(i) Average velocity M_v;
(ii) Average change in velocity M_j;
(iii) Time spent in the adjacent lane M_t;
(iv) Number of overtake maneuvers initiated M_o;
(v) Success percentage of overtake maneuvers M_s.

The goal of the ego vehicle is to maximize the *average velocity* while minimizing the *time spent in the adjacent lane* and *average change in velocity between time steps*, which is used as a metric to evaluate driver comfort. The *number of overtake maneuvers initiated*, and their *success percentage*, are utilized as measures of aggressiveness of the ego vehicle.

1) High-level Optimization Parameters: The behavior of the ego vehicle depends on the tradeoff parameters γ_1, γ_2 and γ_3 in the objective function (16). The effects of parameters γ_1 and γ_3 on the metrics M_v, M_s, and M_t are illustrated in Fig. 5. The parameter γ_1 governs the weightage of the algorithm on maximizing ego vehicle's velocity. Increasing γ_1 up to a certain threshold yields an increase in average velocity and overtaking success. Beyond this point, however, further increase in the value of γ_1 results in an overly aggressive behavior, where the ego vehicle tries to initiate an overtake maneuver at every chance it gets, resulting in a decrease in overtaking success, an increase in the time spent in the adjacent lane, and a decrease in the average velocity. In contrast to γ_1, the parameter γ_3 reflects driver's comfort by restricting abrupt changes in velocity. As expected, increasing γ_3 results in lower average velocity, lower overtaking success and greater time spent in the adjacent lane.

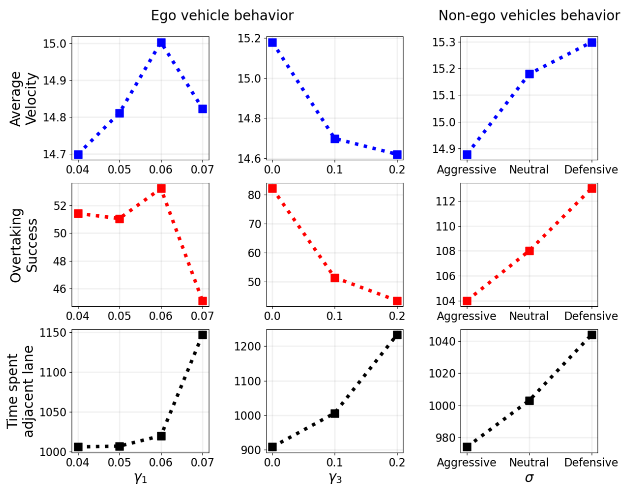

Fig. 5. Algorithm performance with respect to the varying behavior of the ego and the non-ego vehicles

2) Level of Cooperation: Driving imperfections can be modeled by the $Sigma(\sigma)$ parameter in SUMO's Krauss Car-following model [29], and when coupled with varying acceleration and deceleration limits, it gives rise to varying levels of aggressiveness of the non-ego vehicles, as depicted in Fig. 5. In response to aggressive behavior from non-ego vehicles, the ego vehicle attempts fewer overtake maneuvers while spending less time overall in the adjacent lane, resulting in a lower average velocity. In response to defensive behavior from non-ego vehicles, the ego vehicle attempts more overtake maneuvers while spending more time in the adjacent lane, resulting in a higher average velocity.

3) Traffic density: Finally, the behavior of the algorithm in varying traffic densities is presented in Fig. 6. As the number of vehicles in both the lanes decreases, the average velocity increases and the average velocity fluctuations, represented by the red error bars in Fig. 6(a), decreases. These trends seem more pronounced in regards to the vehicles in the original lane because with lower number of leading vehicles, the ego vehicle has to execute fewer overtake maneuvers.

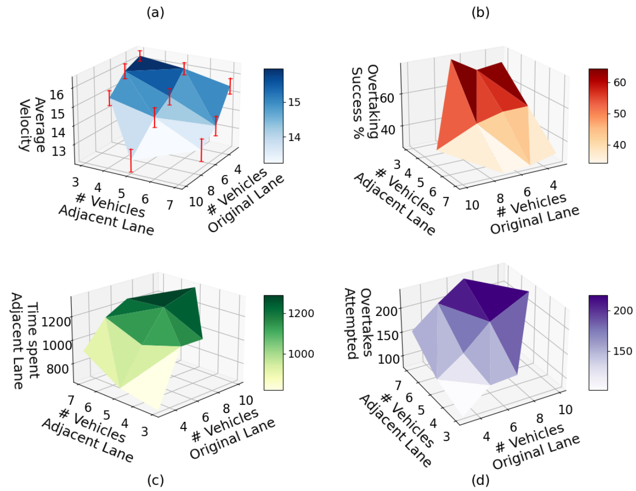

Fig. 6. Algorithm performance with respect to varying traffic density

With decreasing traffic density on the road, the time spent in the adjacent lane decreases (Fig. 6(c)), the overtake attempts decrease (Fig. 6(d)), and their success rate increases (Fig. 6(b)). Note that none of the experiments resulted in a collision.

C. Comparison with Existing Methods

The discussion on the performance of overtaking methods found in the literature often ends with showing that a single overtake maneuver can be successfully performed [6], [9], [18], [19]. In contrast, we have demonstrated the feasibility of the proposed approach without assuming global knowledge, in theory and through simulations. In addition, we have further analyzed the performance of the proposed approach by considering different performance metrics, as explained in Section IV.

V. Conclusion

In this work, a novel mixed-integer model predictive controller, having low computational complexity, was developed to perform autonomous overtaking, while prioritizing safety, in a bidirectional mixed-traffic setting. The ability to retract the overtaking decision after initiating the maneuver was gained through the introduction of a binary decision variable. The intrinsic behavior variability of the observed vehicles was accounted for by the modification of vehicle-dependent safety margins. The operation capability of the method in dense traffic was achieved through an explicit modeling of limited sensing range and occlusion. Finally, the performance of the controller in diverse settings was verified through simulations in the SUMO environment.

Future work would entail a deeper study into the effects of different noise models on the performance of the algorithm. Moreover, the proposed approach could be implemented on a small-scale physical setup to evaluate the robustness of the controller. Finally, more complicated system models could be incorporated in the proposed approach to observe the speed-accuracy tradeoff.

REFERENCES

[1] P. Koopman and M. Wagner, "Autonomous vehicle safety: An interdisciplinary challenge," *IEEE Intelligent Transportation Systems Magazine*, vol. 9, no. 1, pp. 90–96, 2017.

[2] B. Vanholme, D. Gruyer, B. Lusetti, S. Glaser, and S. Mammar, "Highly automated driving on highways based on legal safety," *IEEE Transactions on Intelligent Transportation Systems*, vol. 14, no. 1, pp. 333–347, 2012.

[3] C. Miller, C. Pek, and M. Althoff, "Efficient mixed-integer programming for longitudinal and lateral motion planning of autonomous vehicles," in *2018 IEEE Intelligent Vehicles Symposium (IV)*. IEEE, 2018, pp. 1954–1961.

[4] Y. Kuwata, J. Teo, G. Fiore, S. Karaman, E. Frazzoli, and J. P. How, "Real-time motion planning with applications to autonomous urban driving," *IEEE Transactions on control systems technology*, vol. 17, no. 5, pp. 1105–1118, 2009.

[5] W. Khaksar, K. S. M. Sahari, and T. S. Hong, "Application of sampling-based motion planning algorithms in autonomous vehicle navigation," *Autonomous Vehicle*, vol. 735, 2016.

[6] C.-J. Hoel, K. Wolff, and L. Laine, "Automated speed and lane change decision making using deep reinforcement learning," in *2018 21st International Conference on Intelligent Transportation Systems (ITSC)*. IEEE, 2018, pp. 2148–2155.

[7] M. Kaushik, V. Prasad, K. M. Krishna, and B. Ravindran, "Overtaking maneuvers in simulated highway driving using deep reinforcement learning," in *2018 IEEE Intelligent Vehicles Symposium (IV)*, 2018, pp. 1885–1890.

[8] G. Franze and W. Lucia, "A receding horizon control strategy for autonomous vehicles in dynamic environments," *IEEE Transactions on Control Systems Technology*, vol. 24, no. 2, pp. 695–702, 2015.

[9] P. Falcone, F. Borrelli, J. Asgari, H. E. Tseng, and D. Hrovat, "Predictive active steering control for autonomous vehicle systems," *IEEE Transactions on Control Systems Technology*, vol. 15, no. 3, pp. 566–580, 2007.

[10] J. Suh, H. Chae, and K. Yi, "Stochastic model-predictive control for lane change decision of automated driving vehicles," *IEEE Transactions on Vehicular Technology*, vol. 67, no. 6, pp. 4771–4782, 2018.

[11] S. Dixit, U. Montanaro, M. Dianati, D. Oxtoby, T. Mizutani, A. Mouzakitis, and S. Fallah, "Trajectory planning for autonomous high-speed overtaking in structured environments using robust mpc," *IEEE Transactions on Intelligent Transportation Systems*, vol. 21, no. 6, pp. 2310–2323, 2019.

[12] F. Sulejmani, F. Reiterer, A. Assadi, and L. del Re, "Autonomous overtaking assistant for country road scenarios," in *2020 American Control Conference (ACC)*. IEEE, 2020, pp. 1217–1222.

[13] C. Badue, R. Guidolini, R. V. Carneiro, P. Azevedo, V. B. Cardoso, A. Forechi, L. Jesus, R. Berriel, T. M. Paixao, F. Mutz *et al.*, "Self-driving cars: A survey," *Expert Systems with Applications*, p. 113816, 2020.

[14] S.-L. Lin and B.-H. Wu, "Application of kalman filter to improve 3d lidar signals of autonomous vehicles in adverse weather," *Applied Sciences*, vol. 11, no. 7, 2021. [Online]. Available: https://www.mdpi.com/2076-3417/11/7/3018

[15] S. Thrun, "Probabilistic robotics," *Communications of the ACM*, vol. 45, no. 3, pp. 52–57, 2002.

[16] R. Attia, R. Orjuela, and M. Basset, "Combined longitudinal and lateral control for automated vehicle guidance," *Vehicle System Dynamics*, vol. 52, no. 2, pp. 261–279, 2014.

[17] G. Schildbach and F. Borrelli, "Scenario model predictive control for lane change assistance on highways," in *2015 IEEE Intelligent Vehicles Symposium (IV)*. IEEE, 2015, pp. 611–616.

[18] A. Raghavan, J. Wei, J. S. Baras, and K. H. Johansson, "Stochastic control formulation of the car overtake problem," *IFAC-PapersOnLine*, vol. 51, no. 9, pp. 124–129, 2018.

[19] Y. Gao, F. J. Jiang, K. H. Johansson, and L. Xie, "Stochastic modeling and optimal control for automated overtaking," in *2019 IEEE 58th Conference on Decision and Control (CDC)*. IEEE, 2019, pp. 1273–1278.

[20] R. Lazimy, "Mixed-integer quadratic programming," *Mathematical Programming*, vol. 22, no. 1, pp. 332–349, 1982.

[21] I. Griva, S. Nash, and A. Sofer, *Linear and Nonlinear Optimization: Second Edition*, ser. Other Titles in Applied Mathematics. Society for Industrial and Applied Mathematics (SIAM), 2009.

[22] S. Dixit, S. Fallah, U. Montanaro, M. Dianati, A. Stevens, F. Mccullough, and A. Mouzakitis, "Trajectory planning and tracking for autonomous overtaking: State-of-the-art and future prospects," *Annual Reviews in Control*, vol. 45, pp. 76–86, 2018.

[23] Z. Wang, X. Shi, and X. Li, "Review of lane-changing maneuvers of connected and automated vehicles: models, algorithms and traffic impact analyses," *Journal of the Indian Institute of Science*, vol. 99, no. 4, pp. 589–599, 2019.

[24] B. Arifin, B. Y. Suprapto, S. A. D. Prasetyowati, and Z. Nawawi, "The lateral control of autonomous vehicles: A review," in *2019 International Conference on Electrical Engineering and Computer Science (ICECOS)*, 2019, pp. 277–282.

[25] A. Pierson, W. Schwarting, S. Karaman, and D. Rus, "Navigating congested environments with risk level sets," in *2018 IEEE International Conference on Robotics and Automation (ICRA)*. IEEE, 2018, pp. 5712–5719.

[26] P. A. Lopez, M. Behrisch, L. Bieker-Walz, J. Erdmann, Y.-P. Flötteröd, R. Hilbrich, L. Lücken, J. Rummel, P. Wagner, and E. Wießner, "Microscopic traffic simulation using sumo," in *The 21st IEEE International Conference on Intelligent Transportation Systems*. IEEE, November 2018, pp. 2575–2582.

[27] L. Gurobi Optimization, "Gurobi optimizer reference manual," 2021. [Online]. Available: http://www.gurobi.com

[28] D. V. McGehee, E. N. Mazzae, and G. S. Baldwin, "Driver reaction time in crash avoidance research: Validation of a driving simulator study on a test track," in *Proceedings of the human factors and ergonomics society annual meeting*, vol. 44, no. 20. Sage Publications Sage CA: Los Angeles, CA, 2000, pp. 3–320.

[29] S. Krauss, P. Wagner, and C. Gawron, "Metastable states in a microscopic model of traffic flow," *Phys. Rev. E*, vol. 55, pp. 5597–5602, May 1997.